Packing and Size Determination of Colloidal Nanoclusters

Leonard F. Pease III,*[†,‡] De-Hao Tsai,[†,§] Joshua L. Hertz,[†,#] Rebecca A. Zangmeister,[†]
Michael R. Zachariah,*[†,§] and Michael J. Tarlov*[†]

[†]*Process Measurements Division, National Institute of Standards and Technology (NIST), Gaithersburg, Maryland 20899,* [‡]*Department of Chemical Engineering, The University of Utah, Salt Lake City, Utah 84112,* [§]*Department of Chemistry and Biochemisty and Mechanical Engineering, The University of Maryland, College Park, Maryland 20742, and* [#]*Department of Mechanical Engineering, University of Delaware, Newark, DE 19716*

Here we demonstrate a rapid and quantitative means to characterize the size and packing structure of small clusters of nanoparticles in colloidal suspension. Clustering and aggregation play important roles in a wide variety of phenomena of both scientific and technical importance, yet characterizing the packing of nanoparticles within small clusters and predicting their aerodynamic size remains challenging because available techniques can lack adequate resolution and sensitivity for clusters smaller than 100 nm (optical techniques), perturb the packing arrangement (electron microscopies), or provide only an ensemble average (light scattering techniques). In this article, we use electrospray−differential mobility analysis (ES-DMA), a technique that exerts electrical and drag forces on the clusters, to determine the size and packing of small clusters. We provide an analytical model to determine the mobility size of various packing geometries based on the projected area of the clusters. Data for clusters aggregated from nominally 10 nm gold particles and nonenveloped viruses of various sizes show good agreement between measured and predicted cluster sizes for close-packed spheres.

Introduction

A critical challenge in the development of structured materials for nanotechnology and nanobiotechnology is the lack of readily available, rapid analytical techniques to determine the composition of mesostructured nanoparticles. The dearth of analytical techniques to determine the composition of clusters composed of spherical nanoparticles poses a significant roadblock to the investigation and application of molecular crystals,[1] nucleation of saturated protein solutions,[2] glass transitions,[3] production of photonic crystals,[4,5] viral inactivation, catalyst formulation,[6] and protein aggregation.[2] In this article, we report on a new method to determine the packing and aerodynamic size of colloidal clusters in the nanometer range.

Several established techniques are available to quantify cluster composition and structure, but none are fully satisfactory for those with nanometer length scales. Aggregation of metallic nanoparticles can often be detected by exploiting the phenomena of coupled plasmon resonances using simple optical methods: however, this approach does not provide direct information on aggregate size and structure.[7] Optical microscopy is often applied to determine packing composition of aggregates such as the report by Pine and Manoharan where aggregates formed from micrometer-sized latex spheres were trapped at toluene−water interfaces.[1,8] Similarly, Campbell et al. employ confocal microscopy to observe fluorescently dyed clusters of similarly sized particles.[9] However, both techniques lack resolution and sensitivity for clusters smaller than 100 nm. Alternatively, transmission electron microscopy (TEM), scanning electron microscopy (SEM), or atomic force microscopy (AFM) may be used after samples are deposited on a substrate. Yet, surface forces, often comparable in magnitude to interparticle forces, may disrupt the packing arrangement. These forces can be large enough to drive a four particle cluster initially arranged tetrahedrally into planar configurations with newly formed substrate contacts. Liquid phase deposition processes can also introduce bias into the measurements as hydrodynamic forces in drying drops may lead to aggregation at contact lines similar to the coffee stain effect.[10] These phenomena often hamper TEM analysis, making reliable determination of the packing structure exceedingly difficult. Furthermore, although these microscopies provide stimulating visual images, translating them into quantitative and statistically reliable measurements remains a time intensive and not always straightforward exercise. Dynamic light scattering (DLS) and static light scattering (SLS) methods can overcome many of these limitations and provide rapid, *in situ* analysis of aggregation processes.[2,11] For example, Dai et al. recently used DLS as an

*Corresponding authors' e-mail: pease@eng.utah.edu, mtarlov@nist.gov, mrz@umd.edu.

(1) Yi, G. R.; Manoharan, V. N.; Michel, E.; Elsesser, M. T.; Yang, S. M.; Pine, D. J. Colloidal clusters of silica or polymer microspheres. *Adv. Mater.* **2004**, *16* (14), 1204−1207.

(2) Umbach, P.; Georgalis, Y.; Saenger, W. Time-resolved small-angle static light scattering on lysozyme during nucleation and growth. *J. Am. Chem. Soc.* **1998**, *120* (10), 2382−2390.

(3) Cerda, J. J.; Sintes, T.; Sorensen, C. M.; Chakrabarti, A. Kinetics of phase transformations in depletion-driven colloids. *Phys. Rev. E* **2004**, *70* (1), 011405.

(4) Kim, B.; Carignano, M. A.; Tripp, S. L.; Wei, A. Cluster size analysis of two-dimensional order in colloidal gold nanoparticle arrays. *Langmuir* **2004**, *20* (21), 9360−9365.

(5) Sardar, R.; Heap, T. B.; Shumaker-Parry, J. S. Versatile solid phase synthesis of gold nanoparticle dimers using an asymmetric functionalization approach. *J. Am. Chem. Soc.* **2007**, *129* (17), 5356−5357.

(6) Velev, O. D.; Kaler, E. W. Structured porous materials via colloidal crystal templating: From inorganic oxides to metals. *Adv. Mater.* **2000**, *12* (7), 531−534.

(7) Kim, T.; Lee, C. H.; Joo, S. W.; Lee, K. Kinetics of gold nanoparticle aggregation: experiments and modeling. *J. Colloid Interface Sci.* **2008**, *318* (2), 238−43.

(8) Manoharan, V. N.; Elsesser, M. T.; Pine, D. J. Dense packing and symmetry in small clusters of microspheres. *Science* **2003**, *301* (5632), 483−487.

(9) Campbell, A. I.; Anderson, V. J.; van Duijneveldt, J. S.; Bartlett, P. Dynamical arrest in attractive colloids: The effect of long-range repulsion. *Phys. Rev. Lett.* **2005**, *94* (20), 208301.

(10) Fischer, B. J. Particle convection in an evaporating colloidal droplet. *Langmuir* **2002**, *18* (1), 60−67.

(11) Russel, W. B.; Saville, D. A.; Schowalter, W. R. *Colloidal Dispersions*; Cambridge University Press: New York, 1989.
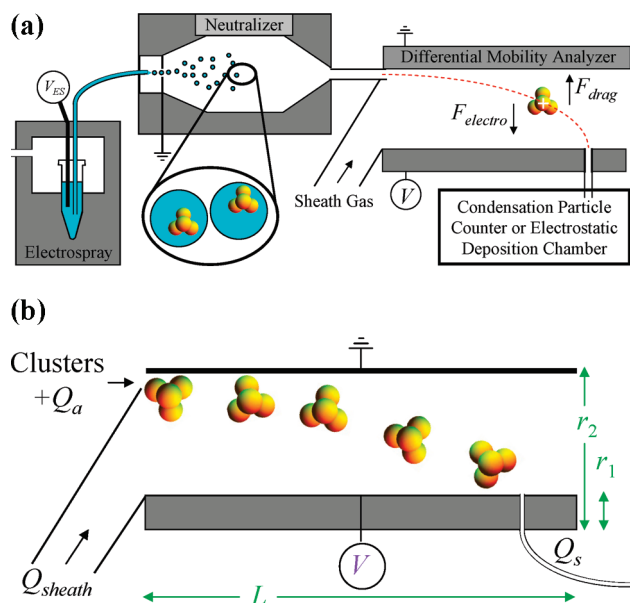
(a)

(b)

Figure 1. (a) Schematic diagram showing the major components of the sample preparation system include an electrospray (ES) to produce highly charged droplets, an electrostatic neutralizer to reduce the charge on the droplet as particles in it dry into clusters, a differential mobility analyzer (DMA) that separates particles based on their charge-to-size ratio, and a condensation particle counter (CPC) to count clusters of a particular size. The trajectory of the particle at terminal velocity is determined by balancing the electrical and drag forces. Once the size of a particular cluster is known, it can be preferentially collected by replacing the CPC with an electrostatic deposition chamber. (b) Schematic displaying the primary variables associated with the flow and geometry of the DMA including the volumetric flow rates of the sheath, Q_{sheath}, aerosol, Q_a, and sampling, Q_s, flows; V is the applied voltage, L ($=$ 4.987 cm) is the length of the analysis chamber, and r_1 ($=$ 0.937 cm) and r_2 ($=$ 1.905 cm) are its inner and outer radii.

indicator of aggregation.[12] However, DLS does not conclusively correlate the size or number of individual particles with the size of an aggregate and cannot resolve individual aggregate concentrations within a multimodal distribution (unless each ratio of sizes exceeds a factor of 3), and clearly distinguishing clusters differing by only a single particle remains challenging, especially for particles less than 30 nm.[13,14] In this paper we report a technique with speed similar to DLS but also with the ability to characterize multimodal distributions and determine the actual number of particles within each cluster with the precision of TEM.

Here we describe the use of differential mobility analysis (DMA) as a rapid and quantitative approach to determine the size and packing of nanoclusters composed of small numbers of colloidal particles. This technique holds the potential to overcome each of the above difficulties, simultaneously providing rapid quantitative analysis, resolution competitive with TEM, and throughput sufficient for statistical reliability (millions of particles per hour). In our apparatus, the clusters are first aerosolized using

electrospray (ES) ionization (see Figure 1).[15,16] The highly charged droplets produced by the electrospray dry as they pass through a neutralizing chamber to reduce the charge distribution to a modified Boltzmann distribution as reported by Weidensohler, leaving the positively charged nanoparticles with only a single net charge ($> 99.999\%$ at 10 nm).[17] Droplet diameter can be easily manipulated by changing capillary diameter or the ionic strength of the solution. The droplets consist predominantly of solvent and electrolytes, typically aqueous ammonium acetate, that evaporate before the dried clusters enter the DMA chamber. Within this chamber, positively charged particles are attracted to a center electrode while being dragged along by a carrier gas. The trajectory of a cluster is established by the balance between electrical and drag forces exerted on the cluster (see Figure 1). The electrical force is varied systematically by stepping through the voltage applied to the center electrode from 0 to −10 kV. Because the charge on the clusters is known and the electrical force is controlled, the only unknown variable in the drag force relationship is the equivalent or mobility diameter of the cluster. Particles with the proper trajectory pass through a collection slit into a condensation particle counter, where they heterogeneously nucleate much larger droplets ($\sim$10 μm) in a saturated butanol environment. The butanol droplets are enumerated as they individually scatter light. This scattered light from individual droplets is converted by a photodetector into voltage pulses, which are then counted as representing individual seed particles (here individual nanoparticles or their agglomerates) passing through per cubic centimeter of gas flow. In other words, the well-known particle size dependence of scattered light plays no role here because all droplets have essentially the same size for number densities used herein. In this manner, a particle size distribution is obtained for the particles and particle clusters.

Although ES-DMA has been used extensively to characterize a wide variety of materials ranging from gold nanoparticles and carbon nanotubes to viruses and virus-like particles, its application has been limited to individual particles and larger aggregates.[4,16,18−23] This is, in large measure, because the drag force relationship returns only a single value of size for particles. An equivalent spherical diameter is most commonly derived. However, more complex treatments can be applied to cylindrical particles with known aspect ratios.[20,23] To date, no theories have been developed to predict or identify the structure of small clusters composed of identical particles based on their precise size measurement by DMA. The work described here addresses that gap. This

(12) Dai, Q.; Liu, X.; Coutts, J.; Austin, L.; Huo, Q. A one-step highly sensitive method for DNA detection using dynamic light scattering. *J. Am. Chem. Soc.* **2008**, *130* (26), 8138−9.

(13) Nie, Z. X.; Tzeng, Y. K.; Chang, H. C.; Chiu, C. C.; Chang, C. Y.; Chang, C. M.; Tao, M. H. Microscopy-based mass measurement of a single whole virus in a cylindrical ion trap. *Angew. Chem., Int. Ed.* **2006**, *45* (48), 8131−8134.

(14) Nguyent, H. V.; Flagan, R. C. Particle Formation and Growth in Single-Stage Aerosol Reactors. *Langmuir* **1991**, *7*, 1807−1814.

(15) Bacher, G.; Szymanski, W. W.; Kaufman, S. L.; Zollner, P.; Blaas, D.; Allmaier, G. Charge-reduced nano electrospray ionization combined with differential mobility analysis of peptides, proteins, glycoproteins, noncovalent protein complexes and viruses. *J. Mass Spectrom.* **2001**, *36* (9), 1038−1052.

(16) Wiedensohler, A. An approximation of the bipolar charge distribution for particles in the submicron size range. *J. Aerosol Sci.* **1988**, *19*, 387−389.

(17) Pease, L. F.; Elliott, J. T.; Tsai, D. H.; Zachariah, M. R.; Tarlov, M. J. Determination of protein aggregation with differential mobility analysis: application to IgG antibody. *Biotechnol. Bioeng.* **2008**, *101* (6), 1214−22.

(18) Pease, L. F.; Lipin, D. I.; Tsai, D. H.; Zachariah, M. R.; Lua, L. H.; Tarlov, M. J.; Middelberg, A. P. Quantitative characterization of virus-like particles by asymmetrical flow field flow fractionation, electrospray differential mobility analysis, and transmission electron microscopy. *Biotechnol. Bioeng.* **2009**, *102* (3), 845−55.

(19) Pease, L. F.; Tsai, D. H.; Zangmeister, R. A.; Zachariah, M. R.; Tarlov, M. J. Quantifying the surface coverage of conjugate molecules on functionalized nanoparticles. *J. Phys. Chem. C* **2007**, *111* (46), 17155−17157.

(20) Pease, L. F.; Tsai, D.-H.; Fagan, J. A.; Bauer, B. J.; Zangmeister, R. A.; Tarlov, M. J.; Zachariah, M. R. Length distributions of single wall carbon nanotubes in aqueous suspensions measured by electrospray-differential mobility analysis. *Small* **2009**, *5* (24), 2894−2901.

(21) Tsai, D. H.; Zangmeister, R. A.; Pease, L. F.; Tarlov, M. J.; Zachariah, M. R. Gas-phase ion-mobility characterization of SAM-functionalized Au nanoparticles. *Langmuir* **2008**, *24* (16), 8483−90.

(22) Tsai, D.-H.; Pease, L. F.; Zangmeister, R. A.; Tarlov, M. J.; Zachariah, M. R. Aggregation kinetics of gold nanoparticles in suspension measured by gas-phase differential mobility analysis. *Langmuir* **2009**, *25* (1), 140−146.

(23) Kim, S. H.; Mulholland, G. W.; Zachariah, M. R. Understanding Ion-Mobility and Transport Properties of Aerosol Nanowires. *J. Aerosol Sci.* **2007**, *38* (8), 823−842.

development is particularly timely because Tsai et al. recently demonstrated ES-DMA as a useful analytical tool to track aggregation of nanoparticles. In this work gold nanoparticle aggregation was measured with ES-DMA, and although the results agreed well with predictions by the theory of Derjaguin, Landau, Verwey, and Overbeek (DLVO)—a theory commonly used to explain colloidal flocculation—it was necessary to use TEM to definitively assign peaks.[22,24,25]

In the remainder of this article, we address the question: Can the DMA be used to determine the cluster size and composition independent of orthogonal techniques, such as TEM? We first review the principles of DMA, emphasizing the role of the drag force and its dependence on the projected area. We then describe an approach to calculate cluster size and compare the calculated sizes with experimental results. We show that this approach accurately predicts the mobility size (i.e., the aerodynamic size measured in the DMA) associated with a cluster and enables the DMA to be used to determine the packing of nanoparticle clusters.

Experimental Section[42]

Cluster Generation. Gold nanoparticles were selected to demonstrate this approach, which is generally applicable to any aerosolizable cluster or aggregate. Citrate-stabilized monodisperse colloidal gold nanoparticles were acquired from Ted Pella, Inc. A suspension containing 1.00 mL of nominally 10 nm gold nanoparticles was centrifuged for 40 min at 13 000 rpm. The visually clear supernatant was removed (typically 0.95 mL) and replaced with 950 μL of 7.9 mmol/L ammonium acetate solution (Sigma, 99.9%, pH 8). Replacing the citrate salts with volatile ammonium acetate minimized the thickness of nonvolatile salt residues that may dry on the surface of the colloid and broaden the detected size distribution.[16,22] This process removed the stabilizing citrate ions and allows for aggregation to induce clustering during ~300 min of incubation prior to analysis.[11,22] The resulting suspension contained individual particles and multiple particle clusters held together by van der Waals forces. Tsai et al. have shown that reducing the electrostatic repulsion between nanoparticles is directly responsible for the aggregation and clustering observed and that this process can be well controlled and quantitatively tuned by adjusting the ionic strength of the solution.[22] If the supernatant was instead replaced with ammonium acetate at 2 mmol/L, significant aggregation was not observed in the ES-DMA size distributions. Approximately 17 min was required from the moment the particles were mixed until the ES-DMA began to record the size distribution.[22] This delay was due to the time needed to insert the sample into the instrument, transit the dead volume within the capillary, establish the electrospray, and begin detecting particles.

ES-DMA Methods. Figure 1a depicts a schematic of our experimental system, consisting of an electrospray aerosol generator (TSI Inc., Shoreview, MN, model #3480), a differential mobility analyzer column (DMA; TSI, Inc., model #3080n), and a condensation particle counter (CPC, TSI Inc., model #3025). Flow handling, interfacing among the instruments, and mobility data reduction were done in-house. The technique has been described in detail elsewhere.[16,21,22,26,27] For particles of unknown sizes, the DMA was rapidly scanned across a broad range of sizes,

and then a more narrow scan with higher resolution and precision was performed. This strategy allowed for detection of subnanometer shifts in particle size.[21,22] The conversion from voltage to mobility size has been described elsewhere for individual spheres and is derived for clusters below.[16,27] Counts in excess of 10 particles/cm³ of flowing carrier gas were considered to be significant, and the noise level within the size distribution remains below this level. Neighboring peaks were distinguished by serial fitting of Gaussian curves as necessary.

Although it was possible to operate the DMA to collect data at equally spaced intervals in mobility space, it was often more convenient to collect data with equal intervals in diameter. Thus, transfer functions of neighboring data points overlapped, and care was taken to not double count particles in the distribution. In other words, because the transfer function had a finite width, specifying the DMA's voltage and flow rates allowed some particles of size $d + \Delta d$ to be collected with those of size d, obscuring the actual size distribution. To remove the influence of doubly counted particles from the size distribution, the charge corrected count was multiplied by $f_{no} = 10.94/d - 29.94/d^2$ as described in detail in the Supporting Information.

The identity of each nanoparticle cluster in the multimodal size distribution was confirmed with transmission electron microscopy (TEM). Particles or clusters of a particular size or mobility were selected by diverting the 1.0 L/min output of the DMA to an electrostatic deposition chamber (TSI 3089). During deposition, the DMA voltage was fixed at a value corresponding to the peak maximum. The electrostatic deposition chamber was operated with a flow rate of 1.0 L/min and an electrostatic potential of −9.8 kV. The size selected particles were deposited onto a carbon film and analyzed with TEM.

Theory. Although previous authors have shown that clusters can be rapidly detected using ES-DMA, corroborating information from TEM or other microscopies has been essential to accurately identify peaks in the size distribution. For example, Tsai et al. tracked the aggregation kinetics of gold nanoparticles into clusters and identified two, three, and four particle clusters (termed dimers, trimers, and tetramers) using electrostatic deposition followed by TEM identification.[22] Similarly, several authors have detected aggregation of virus particles using ES-DMA but have required orthogonal confirmation for peak identification.[28−31] For example, Allmaier et al. recently analyzed tobacco mosaic virus using a variation of ES-DMA (there termed gas-phase electrophoretic mobility molecular analysis or GEMMA) but needed orthogonal confirmation using TEM to correlate the spherically equivalent size measured with particular TMV dimensions.[32] Here we develop the theory essential to identify peaks without orthogonal confirmation, though TEM will be used to confirm the validity of the theory in this study. A more complete explanation is available in the Supporting Information; highlights of the derivation are provided in the remainder of this section.

Within the DMA particles are separated based on their charge-to-size ratio or their aerodynamic mobility, Z. The latter is defined as the ratio of the velocity, U, divided by the electrostatic field, E, necessary to induce it.[33] By controlling both the flow rates and the

(24) Verwey, E. J. W.; Overbeek, J. T. G. *Theory of the Stability of Lyophobic Colloids*; Dover reprint (2001) ed.; Elsevier: Amsterdam, 1948.

(25) Schlüter, H. Theory of colloid stability and particle nucleation kinetics in emulsion polymerization. *Colloid Polym. Sci.* **1993**, *271* (3), 246−252.

(26) Hogan, C. J., Jr.; Kettleson, E. M.; Ramaswami, B.; Chen, D. R.; Biswas, P. Charge reduced electrospray size spectrometry of mega- and gigadalton complexes: whole viruses and virus fragments. *Anal. Chem.* **2006**, *78* (3), 844−52.

(27) Mulholland, G. W.; Donnelly, M. K.; Hagwood, C. R.; Kukuck, S. R.; Hackley, V. A.; Pui, D. Y. H. Measurement of 100 and 60 nm particle standards by differential mobility analysis. *J. Res. Natl. Inst. Stand. Technol.* **2006**, *111* (4), 257−312.

(28) Cole, K. D.; Pease, L. F., III; Tsai, D. H.; Singh, T.; Lute, S.; Brorson, K. A.; Wang, L. Particle concentration measurement of virus samples using electrospray differential mobility analysis and quantitative amino acid analysis. *J. Chromatogr. A* **2009**, *1216* (30), 5715−22.

(29) Thomas, J. J.; Bothner, B.; Traina, J.; Benner, W. H.; Siuzdak, G. Electrospray ion mobility spectrometry of intact viruses. *Spectroscopy* **2004**, *18*, 31−36.

(30) Wick, C. H. Method and System for Detecting and Recording Submicron Sized Particles, July 31, **2007**.

(31) Wick, C. H.; Yeh, H. R.; Carlon, H. R.; Anderson, D. *Virus Detection: Limits and Strategies*; Edgewood Research, Development & Engineering Center: Aberdeen Proving Ground, 1997; pp 1−21.

(32) Allmaier, G.; Laschober, C.; Szymanski, W. W. Nano ES GEMMA and PDMA, new tools for the analysis of nanobioparticles-protein complexes, lipoparticles, and viruses. *J. Am. Soc. Mass Spectrom.* **2008**, *19* (8), 1062−8.

(33) Hind, W. C. *Aerosol Technology*, 2nd ed.; Wiley-Interscience: New York, 1998.

electrostatic potential within the DMA chamber (see Figure 1), particles with a specific mobility can be selected. This instrument mobility, Z^*, is given by

$$Z^* = \frac{\ln(r_2/r_1)}{2\pi VL}\left[Q_{\text{sheath}} + \frac{1}{2}(Q_{\text{a}} - Q_{\text{s}})\right] \qquad (1)$$

where Q_{sheath}, Q_{a}, and Q_{s} represent the volumetric flow rates of the sheath, aerosol, and sampling flows (see Figure 1b), V is the applied voltage, L is the length of the analysis chamber, and r_1 and r_2 are its inner and outer radii.[34] In typical operation, the DMA scans across a range of mobilities by varying the voltage. The remainder of the derivation is focused on determining the mobility at which clusters of a particular composition is equivalent to a specific instrument mobility.

This particle or cluster mobility depends on both the aerodynamic and electrical forces acting on it. The electrical force is given by $F_i = \mu K_{ij} U_j$, where

$$K_{ii} = \frac{3\pi D}{C_{\text{c}}}\delta_{ij} = \frac{3\pi D\delta_{ij}}{1 + K_n[\alpha + \beta\exp(-\gamma/K_n)]} \qquad (2)$$

for a sphere of diameter $D = 2R$, and δ_{ij} is Kronecker's delta.[35] Employing the Cunningham slip correction factor, $C_{\text{c}} = 1 + K_n[\alpha + \beta\exp(-\gamma/K_n)]$ with $\alpha = 1.257$, $\beta = 0.400$, and $\gamma = 1.100$,[36] provides a single expression that holds across the range of Knudsen numbers ($K_n \equiv \lambda/2D$). In the limit of large K_n, Epstein[37] shows that $K_{ii} = (4/\lambda)[1 + (\pi/8)f](\pi R^2)\delta_{ij}$ for a spherical particle with λ representing the mean free path of the molecules inducing the drag ($\sim$66 nm for nitrogen) and f representing the accommodation coefficient typically given as 0.9.[38,39] This expression shows that the translation tensor contains a proportionality to the projected area, πR^2, a fact we exploit below.

The electrical force acting on the particle is given by $F_i = NeE_i$, where N is the number of elementary charges of magnitude e residing on the cluster in an electric field E_i. The number of charges is set within the neutralization chamber as given by Wiedensohler.[17] Equating the electrical and fluid dynamic forces gives $NeE_i = \mu K_{ij} U_j$. This expression may be scaled by choosing the length, $3\pi D/C_{\text{c}}$, as the scale for the translation tensor (see eq 2, middle term) and the scalars U and E as scales for U_i and E_i, respectively. The choice of this scaling is important because it is exact for a sphere, and we assume that shapes of small clusters do not deviate radically from that of a sphere, and also because it is consistent with the traditional form of the aerodynamic mobility of a sphere given as

$$Z \equiv \frac{U}{E} = \frac{NeC_{\text{c}}}{3\pi\mu D} \qquad (3)$$

Then $\bar{U}_i = b_{ij}\bar{E}_{ij}$, where $b_{ij} = (3\pi D/C_{\text{c}})K_{ij}^{-1}$, such that b_{ij} approaches δ_{ij} in the limit of a sphere. There are nine components to this tensor. The translation tensor is symmetric, reducing the number of independent components to six. The tally can be further reduced to three diagonal elements, b_1, b_2, and b_3 (i.e., $b_{ii} = b_i$ and $b_{ij} = 0$ where $i \neq j$), through the use of principal axes, regardless of particle geometry however irregular. These dimensionless mobili-

ties depend primarily on particle geometry. We, therefore, posit that b_i/D can be reasonably approximated as $(\pi/4A_i)^{1/2}$, where A_i is the area of the projection of the particle orthogonal to the ith principal axis.[16] This assumption is exact for a perfect sphere.

As the particle is free to rotate at any moment during its flight through the DMA, collisions between gas molecules and the surface of the particle provide the torque necessary for the particle to sample a variety of orientations, as long as molecules impact anywhere but the center of hydrodynamic stress.[40] A sphere 10 nm in diameter (e.g., an individual gold particle) transiting the DMA in 1 s at standard temperature and pressure should impact $\sim$10[11] gas molecules, most of which can induce a momentary rotation. The mobility observed by the DMA represents an average over all the orientations. To account for them, we average over all possible angles as follows

$$\langle b_{ij}\rangle_r = \int_0^{2\pi}\int_0^{2\pi}\int_0^\pi b_{ij}(\theta,\psi,\phi)P(\theta,\psi,\phi)\,\mathrm{d}\theta\,\mathrm{d}\psi\,\mathrm{d}\phi \qquad (4)$$

where the operator $\langle...\rangle_r$ denotes a rotational average over all three Eulerian angles[40] and $P(\phi,\psi,\theta)$ is the probability of encountering the particle in a certain orientation. When Brownian rotation dominates over shear or electrical alignment,[23] the probability distribution would be expected to be essentially random giving upon normalization, $P(\phi,\psi,\theta) = \sin[\theta]/8\pi^2$. Because only diagonal elements remain and we have averaged over all possible orientations, $\langle b_{ij}\rangle_r = \langle b_r\rangle\delta_{ij}$ such that $\langle b\rangle_r = (b_1 + b_2 + b_3)/3$. Because $\langle b_{ij}\rangle$ is diagonalized, $\bar{U}_i = \langle b\rangle_r\bar{E}_i$, and the average dimensional mobility of the particle becomes

$$\langle Z\rangle_r = \frac{NeC_c\langle b\rangle_r}{3\pi\mu D} = \frac{NeC_c(b_1 + b_2 + b_3)}{9\pi\mu D} \qquad (5)$$

Traditionally, the two mobilities (eqs 1 and 5) may be equated as

$$\frac{NeC_{\text{c}}}{18\sqrt{\pi}\mu}\sum_{i=1}^{3}A_i^{-1/2} = \frac{\ln(r_2/r_1)}{2\pi VL}\left[Q_{\text{sheath}} + \frac{1}{2}(Q_{\text{a}} - Q_{\text{s}})\right] \qquad (6)$$

to obtain the mobility diameter. However, for a nonspherical particle a single length scale does not readily emerge on the left-hand side of this equation for the general case, although one might naturally fall out of a particular case (e.g., the diameter or radius of a cylinder with fixed aspect ratio).[20] We, therefore, devise to predict the mobility size of clusters by ratio, given that the diameter of individual particles can be readily measured. Setting the left-hand side of eq 6 in the limit of a perfect sphere to the left-hand side of eq 6 for the more general (structured) case yields

$$d_n = \left(\frac{\sqrt{\pi}}{6}\sum_{i=1}^{3}A_i^{-1/2}\right)^{-1} \qquad (7)$$

where d_n is the equivalent or mobility diameter of a cluster composed of n particles per cluster.

By way of example, Figure 2 shows the principal projections (on lower right) of a pyramidal structure composed of four spherical particles. The projected areas are $A_1 = A_2 = A_3 = 4(\pi d_1^2/4) - 4A_{\text{ov}}(d_1\sqrt{2}/2)$, where d_1 is the diameter of an individual sphere and the overlapping area, A_{ov}, between two circles is given by

$$A_{\text{ov}}(s) = 2\int_0^{\sqrt{d_1^2 - s^2}/2}\left(-s + 2\sqrt{d_1^2/4 - x^2}\right)\mathrm{d}x \qquad (8)$$

with projected centers separated by distance $s \leq d_1$. With these formulas we calculate explicitly the ratio of the mobility diameter of the cluster size to the diameter of an individual particle composing

(34) Karlsson, M. *Methods to Generate Size- and Compostion Controlled Aerosol Nanoparticles*; Lund, 2004.

(35) Deen, W. M. *Analysis of Transport Phenomena*; Oxford University Press: New York, 1998.

(36) Saucy, D. A.; Ude, S.; Lenggoro, I. W.; de la Mora, J. F. Mass analysis of water-soluble polymers by mobility measurement of charge-reduced ions generated by electrosprays. *Anal. Chem.* **2004**, *76* (4), 1045−1053.

(37) Epstein, P. S. On the Resistance Experienced by Spheres in their Motion through Gases. *Phys. Rev.* **1924**, *23* (6), 710.

(38) Friedlander, S. K. *Smoke, Dust, and Haze*, 2nd ed.; Oxford University Press: New York, 2000.

(39) Li, Z.; Wang, H. Drag force, diffusion coefficient, and electrical mobility of small particles. I. Theory applicable to the free-molecular regime. *Phys. Rev. E* **2003**, *68*, 061206.

(40) Happel, J.; Brenner, H. *Low Reynolds Number Hydrodynamics*; Kluwer Academic Publishers: The Hague, 1983.
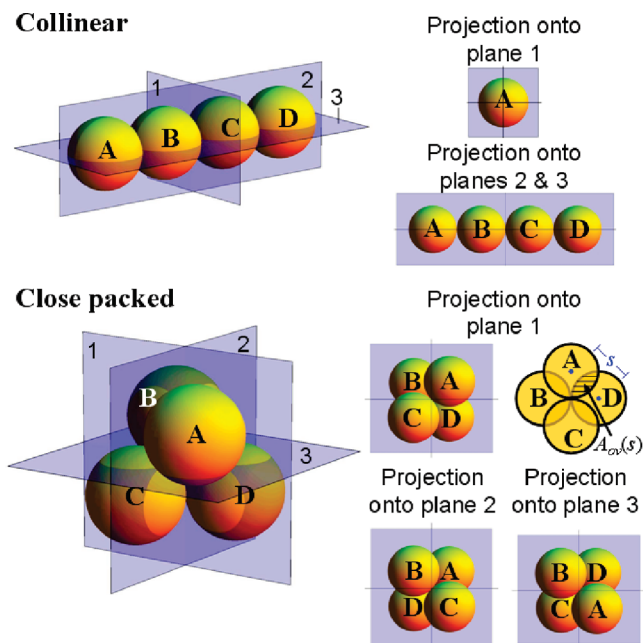
Figure 2. Schematic portraying four-particle clusters with centers arranged either collinearly or close-packed and the planes onto which they are projected. Calculation of the overlap between spheres in the projection uses the variable *s* to denote the distance between projected centers as discussed in the text.

Figure 3. Two typical particle size distributions of nominally 10 nm Au particles, one prior to clustering (dashed) and the other after clustering (solid) induced by adding ammonium acetate (7.9 mmol/L) above the critical salt concentration of ∼7 mmol/L.[22] Peak assignments denote number of particles per cluster. Inset: representative TEM images of small clusters of nanoparticles size selected with the DMA and electrostatically deposited onto TEM substrates (scale bar = 4 nm).

Table 1. Values of d_n/d_1 Calculated for Collinear and Close-Packed Clusters and Values of d_n/d_1 Experimentally Determined from DMA Measured Values of d_n

number of spheres	collinear d_n/d_1	close-packed d_n/d_1	experiment d_n (nm)	experiment d_n/d_1
1	1.000	1.000	11.4 ± 0.2	1.00
2	1.243	1.243	14.4 ± 0.3	1.26 ± 0.05
3	1.392	1.526	17.2 ± 0.4	1.51 ± 0.07
4	1.500	1.809	19.5 ± 0.6	1.72 ± 0.08
5	1.582	1.897	21.1 ± 0.4	1.86 ± 0.07

the cluster, i.e., d_n/d_1. These ratios hold regardless of the size of the clusters so long as Brownian motion continues to rotate them. (Kim et al. consider the electrophoretic and dielectrophoretic forces that could align a 15 nm diameter nanotube and determine orientation effects in a DMA to be negligible for aspect ratios less than 10, as is the case here.[23]) Thus, eq 7 can be used to predict the measured size of a cluster as a function of the number of particles in that cluster, and then that value can be compared to the spherically equivalent size of the cluster measured using the DMA. Though we will compare our peak assignments to TEM, the goal of this research is to provide the more rapid ES-DMA with the ability to characterize the nanoparticle clustering state independent of other techniques.

Results and Discussion

Figure 3 displays two size distributions: one (dashed) acquired from a solution containing individual gold nanoparticles nominally 10 nm in diameter and the other (solid) from a solution of aggregated gold nanoparticles at higher ionic strength (7.9 mmol/L ammonium acetate). Peaks in typical size distributions arise from two sources. The first set of peaks (< 10 nm) corresponds to salt particles that result from the drying of droplets not containing gold particles. The location of these peaks depends on the concentration of nonvolatile salts present in the analyte solution. The second set of peaks (> 10 nm) represents individual gold particles and multiple particle clusters encrusted with nonvolatile salts. The presence of a salt layer explains in part why the individual particle peak in the size distribution appears marginally larger than its nominal size. Figure 3 also highlights the capability of ES-DMA to capture multimodal size distributions of aggregated nanoparticles with a single scan in contrast to comparing separate scans as done previously with DLS or ES-DMA.[12,19] This is a key advance because DLS is not capable of resolving individual aggregate concentrations within a multimodal distribution (unless each ratio of sizes exceeds a factor of 3).

The identity of the particle cluster peaks has been difficult to determine directly from the mobility size distribution alone
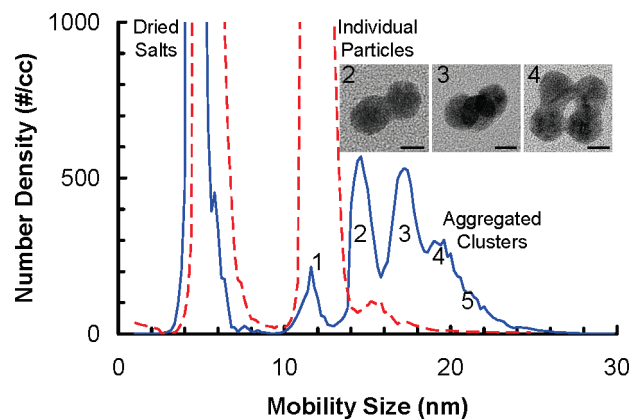
because the mobility size is dependent on the projected area of the particle or particle cluster, not on the total surface area or volume (e.g., the mobility size of a two particle cluster is not simply twice as large as that of a single particle; see Supporting Information). We describe here a modeling approach to identify cluster size from mobility. Briefly, we select a cluster having a specific arrangement of particles of diameter d_1 (see Figure 2). We then determine its principal axes and the minimum projected areas perpendicular to the axes, A_i. We then use eq 7 to determine the mobility size of the cluster, d_n. Table 1 presents the ratio of the two diameters (d_n/d_1) for each cluster composition.

We then consider two limiting cases for the configuration of particles. In the first, the particles are tangent with centers aligned collinearly. Such packing might represent the case for diffusion limited scenarios where the aggregate morphology reflects the first points of contact for each monomer addition.[11] In the second case, we consider a close-packed arrangement. This may be relevant where an incoming particle may sample many possible configurations before selecting the energetically most favorable, i.e., the one with the most contact points.[8] Although we present only two limiting cases, other configurations are possible. For example, a square packing of four particles restrained by right angle geometry has a ratio of $d_n/d_1 = 6/(1 + 2^{3/2}) \approx 1.57$ (see Supporting Information). Thus, clusters with intermediate structures possess sizes intermediate to those found in Table 1.

Because the mobility size depends on the projected area, extended structures (e.g., collinear ones) might be expected to have larger mobility diameters, but we find just the opposite. This can be rationalized by recognizing that particles can remain effectively hidden in extended structures. For example, in a cluster

of four collinear particles, three of the four particles are invisible when viewed along the axis. Thus, close-packed structures display larger projected areas than collinearly packed structures.

The final columns of Table 1 display the dimensional cluster size, d_n, and the ratio of the effective cluster diameter to the individual particle diameter for the experimentally generated clusters (see Figure 1). The uncertainties in the peak locations reported in Table 1 reflect both the repeatability from experiment to experiment (<0.3 nm) and the thin salt layer coating the clusters. The instrument contributes 0.2 nm of uncertainty (full width at half maximum; see Supporting Information) at 10 nm and 0.4 nm at 21.6 nm. Comparison of d_n/d_1 from experiment to that from calculation shows better agreement with the close-packed configurations. This result is not particularly surprising as close-packed structures possess more contact points and are predicted by Lennard-Jones simulations when van der Waals forces govern,[8] as should be the case for electrically stabilized colloids under high salt conditions.[11] Alternatively, the particles may have rearranged into close-packed structures under the influence of capillary forces as the electrosprayed droplet evaporates. In either case, the data tend toward agreement with the ratios for close-packed structures.

The number of particles per cluster was confirmed experimentally by TEM microscopy. The aerosol stream emerging from the DMA was diverted to an electrostatic deposition chamber to capture clusters of a specific size on a TEM grid. The inset to Figure 3 shows typical clusters collected at the maxima. For example, $>90\%$ of the clusters collected with a mobility size of 17 nm contained three distinct particles. The use of TEM microscopy for particle cluster identification is time-consuming and may not truly represent the gas-phase particle packing due to effects of the electrostatically driven impact of the cluster and van der Waals forces between the cluster and the TEM substrate. Our modeling approach extracts the size and preimpact structure of the cluster in the gas phase and does not suffer from lengthy analysis time (<40 min), contact line induced aggregation on substrates (though drying of electrospray droplets might compact extended structures), or post-impact substrate−cluster interactions (e.g., TEM herein).

The analytical method outlined here is not limited to clusters containing five nanoparticles or less but can be applied to much larger clusters both in absolute size and number of constituent particles. For example, commercially available DMAs can size particles up to ∼700 nm, and the largest virus aggregates summarized below were 150 nm in diameter.[31] We note, however, that separation between peaks decreases as the number of particles increases, while the width of the peak remains nearly constant. Pease et al. identify a similar overlap for aggregated proteins as the aggregate size increased.[18] Eventually the peaks overlap and Gaussian fitting techniques become critical to confirming peak location. Estimates of the maximum number of clusters distinguishable by this method may be obtained by comparing the width of Gaussian distributions fit to the data in Figure 3 ($\sigma = 0.7$ nm or $\sigma/d_1 = 0.06$) to a power law fit of the theory for close-packed clusters in Table 1 or Figure 4. Extrapolation suggests that clusters up to 8−25 distinct particles can be distinguished using this method. Nevertheless, as novel synthesis techniques generate increasingly monodispersed nanoparticles, the resolution may improve because heterogeneity in the distribution of nanoparticles composing the cluster represents the primary contribution to peak width.

We finally assert that this technique can be broadly applied and is not limited to gold nanoparticles. Indeed, others have used ES-DMA to characterize individual particles ranging from
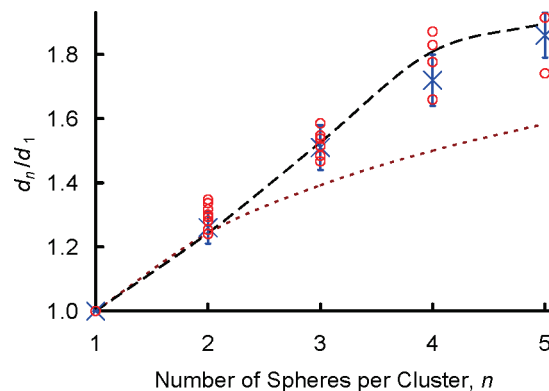

Figure 4. Ratio of the diameter of a cluster, d_n, to the diameter of an individual particle, d_1, versus the number of spherical particles composing the cluster, n, for close-packed (long dash) and collinear (short dash) configurations. Theoretical configurations are compared to experimental results for virus (○) and gold nanoparticle (×) clusters.

metallic nanoparticles to viruses and virus-like particles.[16,19,22] In each case, clusters, where present, can be identified using the individual particle diameter and the corresponding ratio in Table 1. Figure 4 shows cluster sizes determined by several authors for viral aggregates using ES-DMA. The agreement between this data and close-packed structures for seven different viruses (ϕX174,[28] rice yellow mosaic virus (RYMV),[29] MS2,[30,31] alpha virus,[31] Kilham rat virus,[31] murine hepatitis virus (MHV),[31] and adenovirus strain K87)[31] demonstrates the broad impact of this technique. While most of the particle clusters possess d_n/d_1 ratios within the uncertainty (see Table 1) of the close-packed predictions, the viral clusters with the lowest values of d_n/d_1 may represent intermediate structures such as the planar square packing discussed above. Thus, although orthogonal confirmation for ES-DMA is not necessarily required to make this determination, it may be helpful in this particular situation for clusters represented by intermediate values of d_n/d_1. Finally, we note the distinct value of this approach to characterize clusters of biological and bionanoparticles where imaging by TEM can be insensitive due to the low atomic number of samples or cause damage to samples.

Conclusion

In summary, an approach was described to determine the aerodynamic size and packing structure of small clusters of nanoparticles. Good agreement was found between the measured size of gold nanoparticle clusters and predictions for close-packed spheres, and though the current configuration does not have the resolution to distinguish among the continuum of structures intermediate between collinear and close-packed, higher resolution custombuilt instruments have recently been reported that may offer this capability.[41] We also demonstrated DMA as a valuable tool to investigate the structure of nanoparticle clusters (and aggregates more generally) because of its ability to determine size with high resolution. In addition, DMA can rapidly determine the size of multiple particle clusters with minimum perturbation as compared

(41) Ramiro, E.; Ramiro, F.; Sanchez, M.; Lazcano, J. A.; Juan, J. D.; Mora, J. F. d. l. A DMA of inverted geometry for high Reynolds number operation. *J. Aerosol Sci.* **2003**, *Suppl. 2*, 916.

(42) Certain commercial equipment, instruments, or materials are identified in this article to specify the experimental procedure adequately. Such identification is not intended to imply recommendation or endorsement by the National Institute of Standards and Technology, nor is it intended to imply that the materials or equipment identified are necessarily best suited for this purpose.

with other sizing techniques that require deposition of particles onto solid supports.

Supporting Information Available: A complete mathematical derivation of voltage to mobility size conversion for the clusters and the overlap correction, how to determine the principal axes of translation of the cluster, and additional examples of these calculations. This material is available free of charge via the Internet at http://pubs.acs.org.